Presented at the Conference on Air Quality II - Mercury, Trace Elements, and Particulate Matter, McLean, Virginia, September 19-21, 2000.

Recent Observations of Fine Particle Levels in Plumes from a Coal-Fired Power Plant

Stephen F. Mueller* and Robert E. Imhoff
Tennessee Valley Authority
P.O. Box 1010
Muscle Shoals, AL 35662-1010

Abstract

High resolution (~40 meters) measurements of trace gas and particle levels have recently been made within plumes from the Cumberland Fossil Plant operated by the Tennessee Valley Authority (TVA). Plumes from Cumberland, as well as other nearby plants, were intensively studied in the late 1970s. The data were used to estimate $SO_2 \Rightarrow SO_4^{2-}$ oxidation rates.[1,2,3,4] Airborne sampling techniques used in 1998-99 studies provide far more information on plume chemical structure than was possible 20 years ago. The region where photochemistry is active, based on horizontal plume traverses, is small compared to the rest of the plume which is either already chemically mature or not yet chemically active. New data can be used to examine the relationship between photochemically active regions in the plume and changes in particle volume. Also, the effect of turbulent eddies of less than plume-scale on chemical species concentrations (segregation) and, thus, on rapid chemical reaction rates can be examined using the relationship between O_3, NO, and NO_2. In addition, the recent data can be used to compare current sulfate production rates in SO_2-scrubbed plumes with rates measured for the same power plant before flue gas desulfurization (FGD) devices were installed. The data on plume structure and sulfate production are both needed to test models designed to simulate plume chemistry and aerosol production in point source plumes. The accurate simulation of the location and extent of photochemical reaction zones and the degree of segregation are newly measured features that can be used to test model performance. The performance of these models for large point source plumes may have important consequences for large-scale modeling efforts designed to examine source-receptor relationships for fine particles ($PM_{2.5}$) and regional haze.

Introduction

Concern over secondary pollutant formation in plumes from coal-fired power plants has recently motivated renewed research on the chemistry occurring within plumes. New instrumentation with faster response times and measuring additional parameters is providing plume details surpassing those of the previous plume chemistry research. Investigators have focused efforts on improving their understanding of ozone and fine particle formation. There is a critical need for such data to support development of improved conceptual and mathematical plume models. These models, in turn, are expected to be used in large-scale model analyses of pollutant formation and transport. Results from such analyses will be used in developing pollution mitigation strategies for ozone, fine particles ($PM_{2.5}$) and regional haze.

The Tennessee Valley Authority (TVA), the Department of Energy National Energy Technology Laboratory (DOE-NETL), and EPRI recently pooled resources to conduct a multi-faceted study of secondary pollutant formation downwind of a large coal-fired power plant (the 2500 MW Cumberland Fossil Plant, CUF) using state-of-the-art measurement technology. Much of the plume sampling work has been done in conjunction with the field measurement campaigns of the Southern Oxidant Study (SOS), especially during the 1995 and 1999 SOS Nashville intensive field studies. This paper describes analyses of plume structure based on aircraft (helicopter) data collected during the 1998 sampling preliminary to the SOS Nashville campaign.

Plume Structure

In 1998 and 1999, air samples were taken using the TVA Bell 205 helicopter. The gas analyzers on board were similar to those previously described for a 1995 study[5] except for the substitution of a more sensitive SO_2 analyzer (TEI model 43S), and the addition of a Particle Measurement Systems PCASP-100X laser particle size spectrometer and a TSI model 3550 3-wavelength nephelometer. The more sensitive SO_2 analyzer was necessary because the installation of the scrubbers at CUF had reduced the SO_2 emission rate by 95%. The laser particle size spectrometer measured the numbers of particles ranging from 0.1 to 3 μm in size, divided into 16 size range bins. The 3-wavelength nephelometer measured the scattering of light due to particle at red (700 nm), green (550 nm) and blue (450 nm) wavelengths.

NO_x and O_3

In 1995 and again in 1998-99 TVA measured the chemical constituents of plumes from large coal-fired power plants to better understand plume structure and chemistry. These measurement programs are described by Imhoff et al.[6] Techniques were developed and tested for measuring plume structure at high spatial resolution.[7,8] All data were recorded at 1 Hz, with the response of most of the instruments also being about 1 Hz. Because of the slow response of the NO_2 analyzer (caused by mixing in the photolysis cell) all data other than NO_2 were transformed to get synchronous 5-s averages. With a typical aircraft speed of 40 m s^{-1}, this resulted in plume data having a spatial resolution of 200 m. Such resolution provides a detailed view of plume structure and its relationship with the environment. As will be seen later, a data set with 1-s resolution can be constructed by deriving a 1-s NO_2 value using data from the other instruments.

Even before measurements of the 1990s, scientists believed NO_x (=NO+NO_2) plumes from large point sources passed through phases in which the chemical structure changed dramatically.[2] More details are needed, however, to develop computer models that would accurately simulate these phases. The TVA data contribute greatly to refining theories of plume photochemical evolution by the addition of high-resolution measurements of NO_2 and particles.

A brief summary of plume evolutionary phases follows. In Phase I, a fresh, elevated NO_x plume moves downwind, out of contact with the ground. At first, vertical spreading of the plume is limited. In a very unstable atmosphere, the plume may even loop up and down in response to large turbulent eddies in the atmospheric boundary layer. However, within a few kilometers the plume top and bottom boundaries become more diffuse as plume material mixes with the surrounding air. Depending on stability/time-of-day, the typical plume eventually grows vertically so that it extends from the ground upward to near the top of the boundary layer. Vertical concentrations of plume material (at scales of greater than 100 m) become fairly uniform due to turbulent mixing.

Horizontal plume spread is generally slower than vertical in the daytime boundary layer. Thus, plume NO_x becomes mixed with ambient air (including reactive hydrocarbons) most rapidly through vertical plume growth. Ground sources of hydrocarbons (biogenic and anthropogenic) fuel what little Phase I photochemistry that occurs,[8] but the high levels of NO_x are not favorable for ozone production except at the extreme margins of the plume. In fact, plume chemistry is dominated by the NO reaction with O_3 during Phase I to form NO_2 and produce the classic O_3 depression below background levels (Figure 1a). The spatial scale over which this occurs varies according to the size of the plume, with it being larger for larger sources. The CUF plume, illustrated in Figure 1, represents the larger class of NO_x sources. At 21 km downwind the CUF plume is typically still in Phase I.

"Smog potential" (SP), a term used to describe the sum of NO_2 and O_3 mixing ratios, is plotted for all plume traverses in Figure 1. It is a crude measure of the O_3 producing potential of the atmosphere assuming that each NO_2 molecule produced one and only one O_3 molecule. Strictly speaking this is never going to be the case. However, it does illustrate, especially for immature plumes in Phases I and II, that despite O_3 deficits in the plume core a situation exists for significant photochemical productivity.

A transition to Phase II begins just beyond 20-30 km downwind from CUF. Lateral entrainment of volatile organic hydrocarbons, or VOCs, creates narrow zones along plume edges in which the NO_x: VOC

ratio is favorable for O_3 production, termed the photochemical reactive zone. This results in the so-called O_3 "wings" or bulges that are illustrated in Figure 1b as measured 55 km downwind from CUF. The O_3 depression is still found between the wings in a zone where the NO_x:VOC ratio remains too high to support net O_3 production.

Gradually, as a plume continues to spread horizontally it entrains more hydrocarbons and NO_x continues to dilute. Whereas, NO may constitute half of the plume NO_x in Phase 1 (Figure 1a), it drops to less than a quarter of the total NO_x in Phase II (Figure 1b) and is all but gone once Phase III (maturity) is reached. Likewise, NO_x dominates the total odd nitrogen oxide species (NO_y) in Phases I and II, but becomes a minor component once Phase III is reached at around 100 km downwind (Figure 1c). O_3 mixing ratio increases in the plume center in Phase III. This is because reactive hydrocarbons eventually become entrained at sufficient levels to enable the VOC-NO_x photochemistry to dominate over the simple NO-NO_2-O_3 photostationary reactions that create a pseudo-equilibrium early in plume growth. In a mature plume O_3 in the center eventually increases to the point where it exceeds O_3 outside the plume creating "excess" O_3 and merging with the wings of Phase II. At this point, the NO_x fuel is exhausted and further net ozone production is ended. From this point a plume continues to diffuse, mix with other source plumes, and lose some of the ozone that has been produced through deposition to the ground. The plume becomes indistinguishable as a separate entity at distances well beyond 100 km downwind, depending mainly on meteorology.

A photochemical reactive zone (PRZ) occurs at those locations in the plume where the NO_x:VOC ratio is favorable for production of O_3. Outside of this region, most of the NO_x has already been converted to NO_z (=NO_y-NO_x) leaving no fuel for the continued production of O_3. Nearer the center of the plume, NO_2 is concentrated enough that it scavenges most of the OH^{-1} radicals, producing HNO_3 but not ozone. The chemical signatures of the PRZ, plume core and plume periphery are illustrated in O_3-NO_y space (Figure 2) using data collected in the CUF plume. Along the extreme edges (periphery), O_3 and NO_y (<12 ppb) are near background levels. A PRZ is encountered when NO_y, enriched by NO_2, increases along with O_3 which is being produced. In the plume core, with NO_y typically >20 ppb, NO is a major component and O_3 declines due to its titration with NO.

The PRZ is an idealized concept. Spatially, it is dispersed in pockets throughout much of the plume due to inhomogenous mixing. This issue is dealt with in greater detail in the section on turbulence effects.

Particles

Particles in the plume of a coal-fired boiler are of two main types. Primary particles are those that are formed either prior to or soon after (< 5 minutes) emission. An example of the latter are sulfuric acid droplets that are formed due to the condensation of SO_3 gas present in the exhaust. Secondary particles are those that form due to chemical and physical processes that occur in the atmosphere more than 5 minutes after emission.

Primary particles in the CUF plume were mainly of sizes from 0.1 to 0.14 μm in diameter, due mostly to sulfuric acid aerosols. This can be determined by examining a plot of particle numbers versus plume NO_y. An example is given in Figure 3 for a plume traverse on 25 August 1998 at 21 km from CUF. The 16 particle size bins have been lumped into three groups according to the observed tendency to vary with NO_y. The first group, A, encompasses the smallest size bins—1-3, 0.12- 0.14 μm in diameter. Group A particles increase linearly with NO_y in the plume, suggesting that they are emitted in proportion to NO_y. These particles are actually formed a short distance downwind after emission. Particles in the second group, Group B—bins 4-7, 0.14-0.4 μm diameter—do not increase with increasing NO_y, suggesting that they originate from outside the plume. Particles in the third size range, Group C—bins 8-10, diameters of 0.4-0.9 μm—actually decline with NO_y. A hypothesis for this behavior will be described later. Group C particles are large enough to be efficient scatterers of visible light, while those in the smallest group are not. Because only the smallest particles are present in the plume in numbers above that in the background, it follows that the net visual effect of plume particles at 21 km downwind is no significant increase in light scattering above that in the ambient air.

Secondary particles are formed by the oxidation of SO_2 and NO_x present in the plume. The SO_2 chemistry is related to the NO_x/ozone chemistry in that both depend on the action of OH^{-1} radicals. Secondary nitrate particles can also form in well-aged plumes, but their presence is strongly dependent on temperature, the availability of ammonia, and the abundance of sulfate. These secondary particles are generally of a size that is efficient at scattering light and are, therefore, important from a regional haze perspective.

Effect of Turbulence on Photochemistry

For a non-linear process such as the formation of NO_2, the chemical reaction rates depend on both the gradual change in time of the average concentration and the short-term, instantaneous fluctuation of concentrations about the average.[9] These short term fluctuations depend upon the frequency and size of the eddies, relative to the overall plume size, with lifetimes on the order of a few minutes. NO_2 is formed when a plume containing NO mixes with ambient air containing O_3:

$$NO+O_3 \Rightarrow NO_2 + O_2 \quad (1)$$

Reaction (1) has a rate constant, k_1, that is approximately 4×10^{-4} $ppb^{-1}s^{-1}$ at 20 C. NO_2 is also formed by the reaction of NO with O_2. This reaction accounts for much of the NO_2 present at the time of emission. NO_2 in the ambient air is photo-dissociated by absorption of ultraviolet (UV) radiation which yields NO and O_3 according to

$$NO_2 + O_2 \Rightarrow NO + O_3 \quad (2)$$

This reaction has a rate constant, k_2, that is dependent on the intensity of solar radiation, and ranges between 0 at night to about $9 \times 10^{-3}s^{-1}$ at noon at the latitude (36° N) and for the time period (July-August) of these studies.

After about 10 minutes of transport, the time-scale of mixing (0.6x transport time in minutes[9]) is long relative to the time scale of reactions (1), 1-30 s, and (2), 3-6 minutes. This produces a local state of equilibrium between NO, NO_2 and O_3 in the plume. Figure 4 illustrates this by comparing the measured NO_2 mixing ratio, $[NO_2]_{ob}$, to that calculated ($[NO_2]_{cp}$) from the values of k_2, $[O_3]_{ob}$ and $[NO]_{ob}$. Here $[NO_2]_{cp}$ will be referred to as photostationary NO_2. Values of $[NO_2]_{ob}$ and $[NO_2]_{cp}$ at 21 km downwind agree almost exactly on the 5-s time resolution plot. This agreement indicates the potential for a 1-second NO_2 observation, based on this technique, under conditions where RO_2 chemistry effects are small. Figure 5a provides an idealized view of a plume cross section in a Phase-1 plume with high $[NO_x]$ in the plume core declining gradually and mixing with ambient air containing high $[O_3]$. Over a one-hour averaging time this is a fair representation of the dynamics of the plume and is the basis for the traditional Gaussian plume distribution. However, the plume chemistry depends not on the long term average conditions but rather on the local conditions within zones of mixing. On an instantaneous basis, illustrated in Figure 5b, the mixing occurs in a chaotic way with high [NO] occurring in localized pockets throughout the plume depicted in Figure 5b. After emission from the stack the flue gas is broken up by turbulence into parcels which consist of undiluted exhaust gas surrounded by other parcels diluted with ambient air.

The production of NO_2 through reaction (1) in the plume depends upon the chemistry at that point in the plume. Since the reactions are fast relative to the mixing and the mixing is non-uniform, a situation arises in which the calculated rate of NO_2 production depends upon the averaging time chosen. The actual integrated rate of production of NO_2 across the plume is given by

$$PNO_2 = \int k * NO_i * O_{3_i}$$

which is approximated, using the measured data, by

$$PNO_2 = \sum_{i=1}^{n} k * NO_i * O_{3_i}$$

in which the sum is based on all discrete in-plume measurements. The calculated rate of NO_2 production, integrated across a plume cross section, will vary with averaging time because of inhomogeneities in plume constituents. These inhomogeneities can lead to an inappropriate matching of [NO] and [O_3]. If NO_2 production is proportional to the product of [NO] and [O_3], then the integrated NO_2 production rate must be computed from $\Sigma\{[NO][O_3]\}$. A model that does not properly simulate the inhomogeneities will compute an integrated NO_2 production rate from the product $\Sigma[NO] \times \Sigma[O_3]$, which is clearly not the same result.

The effect of this in a model can be illustrated by varying the interval used to average the measurements. To illustrate this, the averaging time for measured single plume traverses at 21, 56, and 110 km on 25 August 1998 has been varied from 5 s to 60 s. At each distance, the sum of NO and O_3 concentrations across the plume are the same for all averaging times. A 30-s averaging time for the CUF data set yields a cross wind plume resolution of 1000 m. The plume at about 20 km downwind is about 12 km wide, so 30 s is about the same resolution as a plume model which divides the plume into 10 cross wind segments. The integrated NO_2 production rate for reaction (1) was then calculated for each averaging time. Results are plotted in Figure 6. The greatest effect of longer averaging times is at the closest distance. This is expected because the plume is less homogeneous close to its source.

At 21 km, even if a model with 1 km cross wind resolution produces the correct average concentrations of NO and O_3 across the plume, it will estimate an integrated NO_2 production rate of 24 ppb s^{-1} instead of 16 ppb s^{-1}; an overestimate of 50%. Over a period of several model time steps, excess NO_2 will build up in the model until a new photoequilibrium is reached in the model that is not representative of the true mass of NO_2 in the plume. This distortion of the photochemistry is one rationale for developing models, such as SCIPUFF,[10] that treat explicitly the effect of turbulent concentration fluctuations on chemical kinetics.

For any given averaging time, the plume integrated production rate of NO_2 is greater closer to the stack. This is a result of declining [NO] with distance caused by the conversion of NO_x to NO_z. The representation of the cross wind structure of a plume has been shown to be important to the accurate representation of the chemistry for the relatively fast reaction (1). The next section examines the data for the oxidation of SO_2 to see what cross wind structure occurs and what this implies about the underlying chemistry.

Sulfate Production

In the gas phase, SO_2 is oxidized to SO_3 by OH^{-1} radicals A series of reactions leads to the formation of sulfuric acid (SULF), the precursor of particulate sulfate. The overall reaction can be represented as:

$$HO + SO_2 \Rightarrow SULF + HO_2$$

The overall reaction rate constant of this chain is 3×10^{-31} cm^3 s $molecule^{-1}$.[11]

This rate is about one tenth of the rate for OH^{-1} reacting with NO_2 (2.6×10^{-30} cm^3s $molecule^{-1}$). The [NO_2] in the plume is significantly above [SO_2] at 21 and 55 km at all locations except the outermost edges. The NO_2 will remove most of the available OH^{-1} due both to the higher reaction rate and the higher [NO_2]. This will limit the production of SULF in the plume to the edges of the plume where NO_2 is much less. By the time the plume reaches 110 km [NO_2] has fallen below [SO_2] for all [NO_y] below 12 ppb, which is most of the plume. Thus, SULF formation is expected to occur primarily on the periphery of the plume for most of its chemically active lifetime, then spread inward toward the end of Phase 3.

A method is needed to examine sulfate concentrations on a fine spatial scale to verify expectations regarding sulfate production. It is as yet not feasible to measure sulfate aerosols on the same time scale as is now routinely done for gaseous species. There are techniques that can measure sulfate aerosols continuously[12] from grab samples (impractical for determining detailed cross plume structure)[13] or with an averaging time of as little as 5 minutes.[14] However, these methods are not adequate to distinguish small-scale cross wind

features. Secondary sulfate aerosols have been found in previous studies [15] to be about 0.2 – 0.8 μm in diameter.

Quantities of particles in this size range can be measured with the PCASP-100X probe and light scattering can be measured with a nephelometer. The approach taken here is to examine the small scale structure of secondary aerosols by identifying changes in particle numbers for the various size bins during a plume traverse. This information is then compared to the changes in other species. In particular, NO_y and SO_2 data were used to distinguish the boundaries of the plume, NO_x, NO_z, and O_3 data were used to determine the chemical state of the plume at each cross wind location. High volume filter measurements of the plume particles during this study show that at about 85% of the excess particles in the plume are in the form of sulfates. Because the majority of secondary particles are SO_4^{-2}, the variation of particle volume in the 0.2 to 0.8 mm size range mainly reflects the variation in the secondary SO_4^{-2} in the plume. Observation of particles in this size range allows an indirect means of examining the variation of the SO_4^{-2} at a scale of 200 m within the plume. This information is used here in a qualitative fashion to identify the location of the particle formation within the plume cross section.

In the prior discussion of Figure 3, a distinction was made between primary and secondary plume particles and the sizes at which they occur. Particle size data from plume traverses, represented in Figure 3 (a-c), at different downwind distances can reveal useful information about particle formation processes. At 21 km, the plume has traveled about 0.75 hour downwind of the stack. In the stack, $[NO_2]$ is about 5% of $[NO_x]$ and the $[SO_2]$ is about 10% of $[NO_x]$. Additional NO_2 will be rapidly formed at the edges of the plume by reaction (1), limiting the time for which $SO_2 > NO_2$. It follows, from previous reasoning, that SULF formation other than at plumes edges is not expected at 21 km. However, Figure 3 shows an apparently monotonic decrease of particle counts in Group C with increasing NO_y. This is not consistent with the expected pattern of SULF formation in the plume, which would yield constant Group C numbers across the entire plume. Either SULF formation is occurring early or the particles in this size class are forming from another mechanism. For example, nearer the plume edge some of the Group A particles may grow to a slightly larger size due to increased availability of water vapor in a humid ambient environment.

Particle numbers are plotted for a traverse at 56 km in Figure 3b. The primary particles in Group A are still linearly associated with NO_y, though the slope has increased. Particle number concentrations are compared to SO_2 to examine whether this change in the particle-NO_y relationship is due to particle production or to loss of plume NO_y.[8] This comparison is useful because SO_2 is removed from the plume more slowly than NO_y. The slopes of the Group A particle numbers versus SO_2 for 21, 56, and 110 km are 500, 750, and 700 particles per ppb SO_2, respectively. The increase in the slope of particle numbers between 21 and 56 km is greater than can be explained by loss of SO_2 at a rate of about 4% per hour.[2,3,7] This increase is probably due to growth of particles below the lower size limit of the particle size spectrometer into measurable size. The number of particles in bins 3-8 (Group B) now exhibit a small increase with NO_y. The number of particles in bins 8-10 (Group C) decline with increasing NO_y more rapidly than at 21 km. The decline still appears to be linear with NO_y and is not localized to the edge of the plume.

At 110 km, shown in Figure 3c, the particle numbers of all three groups increase with NO_y. The plume is nearly mature, with little NO except at the plume core. Both the Group A and the Group B particles increase linearly with NO_y. The Group C particles increase with NO_y up to 12 ppb, then level off for higher NO_y. This pattern is consistent with the expected formation of SULF, described previously, on the edges of the plume.

Figure 7 shows several species versus $[NO_y]$. $[SO_2]$ is of about the same magnitude as $[NO_2]$ up to an $[NO_y]$ of about 12 ppb. This is near the point at which the ozone stops increasing with increasing NO_y and begins to decrease due to titration with NO. The volume of 0.1-1.0 μm particles is also plotted versus $[NO_y]$. This exhibits behavior much like the particle numbers in Group C in the previous figure. The particle volume increases from the edge of the plume to an NO_y of about 12 ppb, then is approximately constant. This pattern is consistent with the production of SULF taking place in the PRZ in the plume in the same manner as the production of O_3.

An estimate of the SO_2 conversion rate can be made by assuming that all of the additional excess volume in the plume is due to conversion of SO_2 to $(NH_4)_2SO_4$. To the extent that other processes such as the formation of $(NH_4)HSO_4$ or aerosol nitrate contribute to the excess volume, the current estimate will be biased high. Since $(NH_4)_2SO_4$ particles are known to be small in diameter,[15] only particles less than 0.6 μm are included. In 1998, the average excess volume of the aerosols (up to 0.6 μm) in the plume was 2.6, 1.6, and 2.1 $\mu m^3/cm^3$ at travel times of 0.75, 3, and 8 hr from the source, respectively. Assuming that the entire volume consists of $(NH_4)_2SO_4$, each volume unit (1 $\mu m^3/cm^3$) contains $8.1x10^9$ SO_4^{2-} ions[2]. Average excess SO_2 concentrations were 4, 1.7, and 1 ppbv at these distances, respectively. Ground-based measurements performed in 1978 by McMurry et al.[3] indicated excess volume of 9.3 and 18.4 $\mu m^3/cm^3$ at 2.2 and 5 hr from the source with concurrent SO_2 levels of 72 and 34 ppbv[2].

Figure 8 presents the particle volume-derived SO_2 to SO_4^{2-} conversion rate for the 1978 and 1998 studies. The rate was calculated using the method described by Meagher et al[4]. The estimated upper limit of the conversion rate for the 1998 data is 0.0437 h^{-1} with a 90% confidence interval of ±0.0358 h^{-1}. The conversion rate for the 1978 McMurry data was estimated to be very similar ($k = 0.0443h^{-1}$). The later value is also consistent with the estimate made by Gillani et al.[2] based on continuous airborne measurements of SO_2 and sulfate performed at the same distance on the same day in 1978. Gillani et al. calculated SO_2 to sulfate conversion rate to be in the range of 0.009 and 0.035 h^{-1}. The present estimates slightly exceed the high end of that range. A comparison of the rates in 1978 and 1998 suggests that the recent reduction in SO_2 emissions from CUF has likely been accompanied by a roughly proportional reduction in the amount of SO_4^{-2} formation during plume dispersion.

Implications for Plume Modeling

Plume models must be able to reproduce the spatial relationships of the plume chemical constituents involved in O_3 and SULF production if they are going to accurately simulate the processes important in determining the productivity of plumes for these species. The segregation of species involved in the chemical reactions—with OH^{-1}, VOCs, and O_3 having to diffuse into the plume from outside—creates a dynamic situation in which mixing processes cannot be ignored.

Early plume models did not provide for this level of detail. Although they did show limited skill in delaying plume photochemical production, they still failed to consider the high degree of inhomogeneity known to exist. As a result the early models failed to accurately reproduce plume O_3 productivity consistent with observations. Newer models, such as SCICHEM, have taken the next step in trying to more explicitly consider the turbulent inhomogeneity of a plume and the effect of this process on plume chemistry. Early results are encouraging,[10] but more model comparison with actual plume data are needed to understand how well models like SCICHEM perform under a variety of meteorological and chemical states.

Failure of models to properly consider the factors influencing ozone productivity in point source plumes will continue to provide regulatory authorities with inaccurate guidance on the effectiveness of mitigation strategies based in part on the models. Such guidance will, until models are sufficiently improved, place greater emphasis on benefits associated with point source emission controls over non-point source controls. It is hoped that new modeling systems like Models-3, with its modular design and more advanced embedded plume models, will provide the framework needed to test and evaluate a variety of plume modeling approaches. This is the type of environment that is necessary for promoting significant plume model improvements.

References

1. Meagher, J.F.; Stockburger, L.; Bailey, E.M., and Huff. O., The Oxidation of Sulfur Dioxide to Sulfate Aerosols in the Plume of a Coal-fired Power Plant, *Atmos. Environ.*, 1978, 12, 2197-2203.

2. Gillani, N.V.; Kohli, S., and Wilson, W.E., Gas to Particle Conversion of Sulfur in Power Plant Plumes – II. Parameterization of the Conversion Rate for Dry, Moderately Polluted Conditions, *Atmos. Environ.*, 1981, 15 2293-2313.
3. McMurry, P.H.; Radar, D.J., and Stith, J., Studies of Aerosol Formation in Power Plant Plumes – Implications for chemical conversion mechanisms, *Atmos Environ.*, 1981, 15, 2315-2327.
4. Meagher, J.F.; Stockburger, L.; Bonanno, R.J.; Bailey, E.M., and Luria, M., Atmospheric Oxidation of Flue Gases from Coal-Fired Power Plants – A Comparison Between Conventional and Scrubbed Plumes, *Atmos. Environ.*, 1981, 15, 749-762.
5. Luria, M.; Valente, R.J.; Gillani, N.V.; Tanner R.L.; Imhoff, R.E.; Mueller, S.F., and Meagher, J.F., The Evolution of Photochemical Smog in a Power Plant Plume, *Atmos. Environ., 1999, 33*, 3023-3036.
6. Imhoff, R.E.; Tanner, R.L.; Valente, R.J., and Luria, M., The Evolution of Particles in the Plume from a Large Coal-Fired Boiler with Flue Gas Desulfurization, *J. Air & Waste Manage. Assoc*., 2000, 50:12-07-1214.
7. Imhoff, R.E.; Luria, M.; Valente, R.J., and Tanner, R.L., NO_y Removal from the Cumberland Power Plant Plume, *Atmos. Environ.*, Accepted for publication 2000.
8. Luria, M.; Tanner, R.L.; Imhoff, R.E.; Valente, R.J.; Bailey, E.M., and Mueller, S.F., Influence of natural hydrocarbons on ozone formation in an isolated power plant plume, *J. Geophysical Research*, 2000, V105, No. D7, 9177-9188.
9. Janssen, L.H.; Niewstadt, F.T.M., and Donze, M., Timescales of Physical and Chemical Processes in Chemically Reactive Plumes, *Atmos. Environ*., 1990, V24A, No. 11, 2861-2874.
10. Karamchandani, Prakash; Santos, L.; Sykes, I.; zhang, Y.; Tonne, C., and Seigneur, C., Development and Evaluation of a State-of-the-Science Reactive Plume Model, *Environ. Sci. Techno.*, 2000, 34, 870-880.
11. National Acid Precipitation Assessment Program. The Regional Acidic Deposition Model and Engineering Model, Report 4 (Appendix 4). In *Acid Deposition: State of Science and Technology*; Irving, P.M., Ed; Office of the Director: Washington, DC, 1990; Vol. 1: Emissions, Atmospheric Processes, and Deposition.
12. Garber, R.W.; Daum, P.H.; Doering, R.F.; D'Ottavio, T., and Tanner, R.L., Determination of Ambient Aerosol and Gaseous Sulfur Using a Continuous FPD – III. Design and Characterization of a Monitor for Airborne Applications, *Atmos. Environ*., V17, No. 7 1381-1385.
13. Hobbs, P.V.; Heff, D.A.; Eltgroth, M.W., and Radke, L.F., Evolution of Particles in the Plumes of Coal-Fired Power Plants – I. Deductions from Field Measurements, *Atmos. Environ*., 1979, V13, 935-951.
14. Hering, S.V., Private Communication, 1999.
15. Hobbs, P.V., and Hegg, D.A., Sulfate and Nitrate Mass Distributions in the Near Fields of Some Coal-Fired Power Plants, *Atmos. Environ*., 1982, 16, 2657-2662.

Acknowledgements

The authors are indebted to many individuals whose efforts made it possible to do the work described here. Special thanks are given to Roger Tanner for his insight into plume chemistry, Ralph Valente for his tireless work in developing and maintaining a complex aircraft measurement system, and Lynn Humes for her work in processing the raw data for analysis. This work was supported by the TVA Public Power Institute, the DOE National Energy Technology Laboratory, and EPRI. Mention of commercial instruments does not constitute an endorsement.

(a)

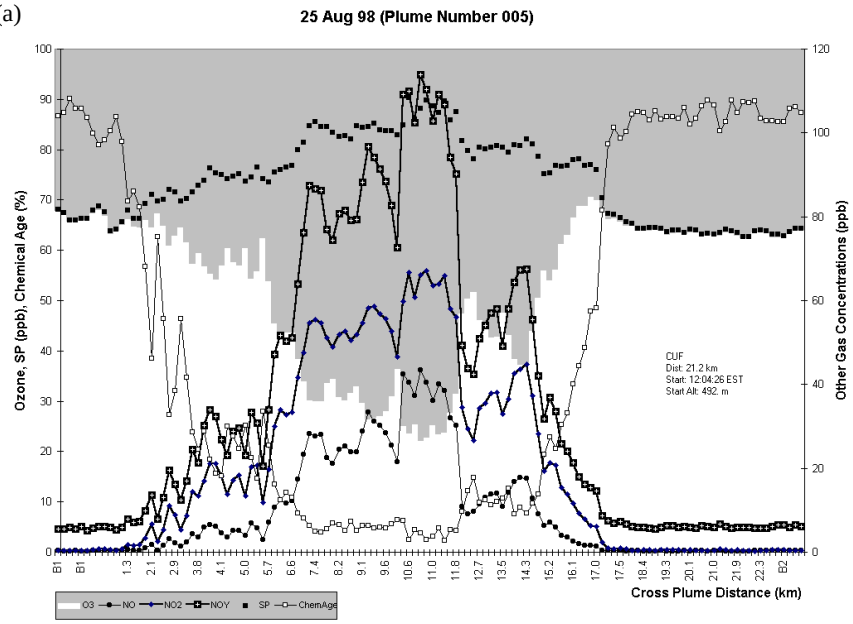
25 Aug 98 (Plume Number 005)
Ozone, SP (ppb), Chemical Age (%)
Other Gas Concentrations (ppb)
Cross Plume Distance (km)
CUF
Dist: 21.2 km
Start: 12:04:26 EST
Start Alt: 492. m
O3
NO
NO2
NOY
SP
ChemAge

(b)

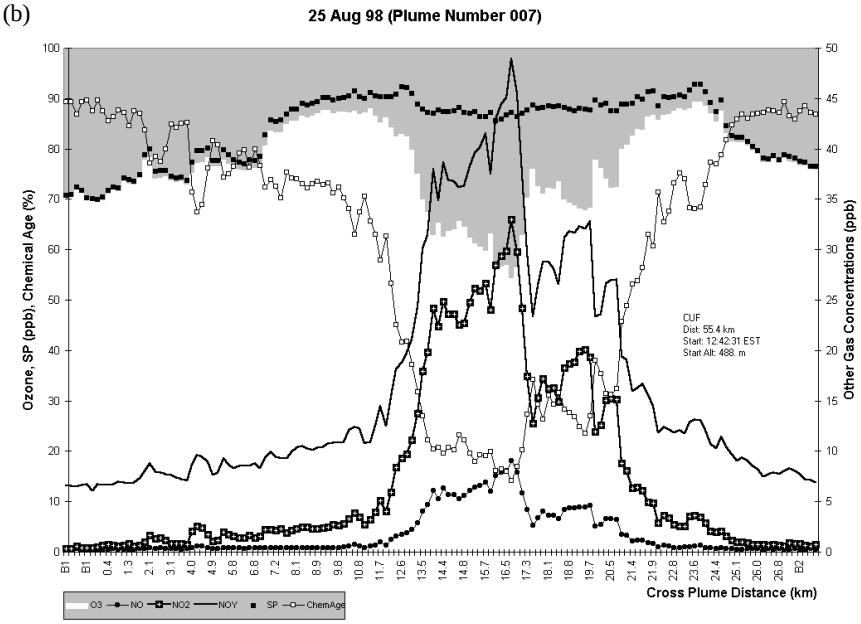
25 Aug 98 (Plume Number 007)
Ozone, SP (ppb), Chemical Age (%)
Other Gas Concentrations (ppb)
Cross Plume Distance (km)
CUF
Dist: 55.4 km
Start: 12:42:31 EST
Start Alt: 488. m
O3
NO
NO2
NOY
SP
ChemAge

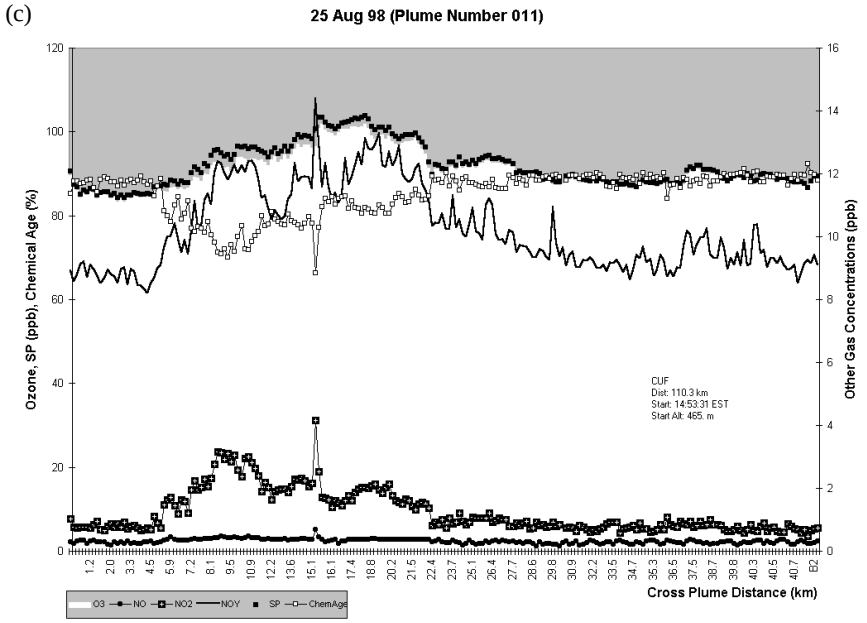

Fig. 1. CUF cross-plume measurements of photochemical constituents at three downwind distances: (a) 21 km, (b) 55 km, and (c) 110 km. Ozone mixing ratios are shown using vertical white bars (plot frame background is gray); all other parameters are shown by lines and/or symbols. Note that the scales of the left and right ordinates vary for the different graphs. SP denotes "smog

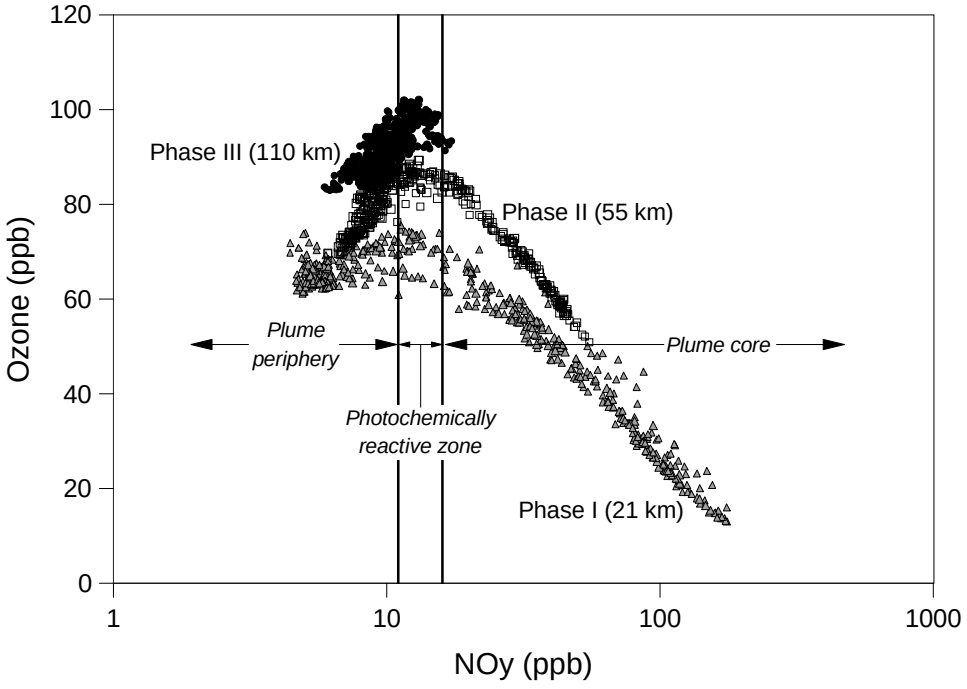

Fig. 2. Chemical characterization of zones in a plume according to typical levels of NO_y and O_3.

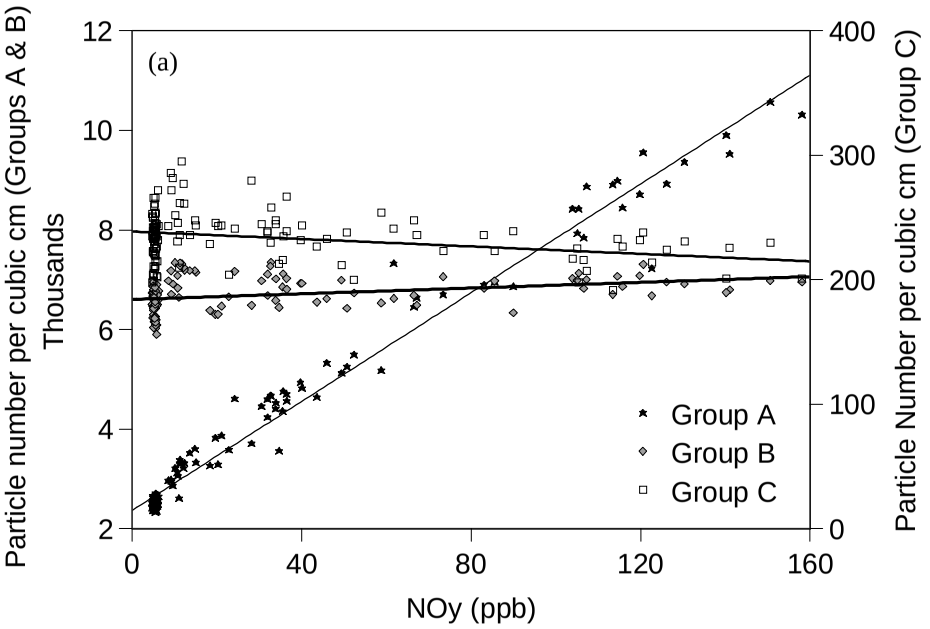
(a)
Particle number per cubic cm (Groups A & B)
Thousands
Particle Number per cubic cm (Group C)
NOy (ppb)
Group A
Group B
Group C
12
10
8
6
4
2
400
300
200
100
0
0
40
80
120
160

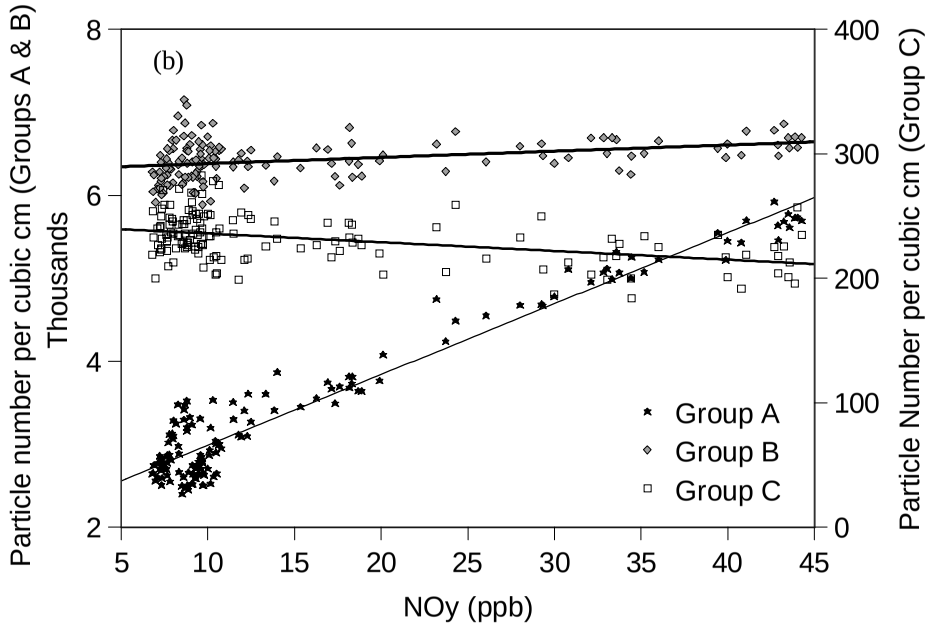
(b)
Particle number per cubic cm (Groups A & B)
Thousands
Particle Number per cubic cm (Group C)
NOy (ppb)
Group A
Group B
Group C
8
6
4
2
400
300
200
100
0
5
10
15
20
25
30
35
40
45

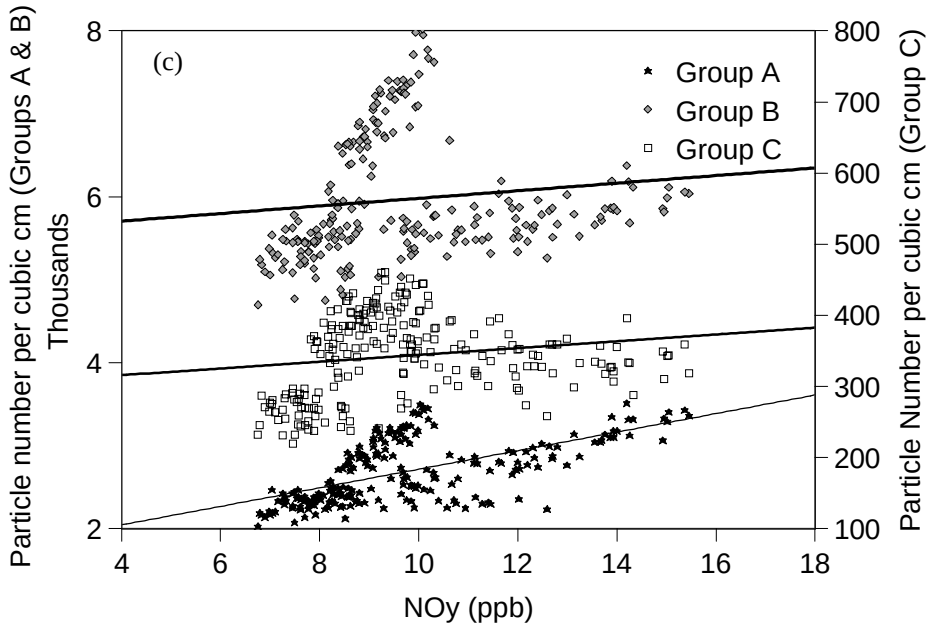

Fig. 3. Measured plume particle number concentrations versus NO_y by size category for (a) 21 km, (b) 56 km and (c) 110 km downwind on 25 August 1998.

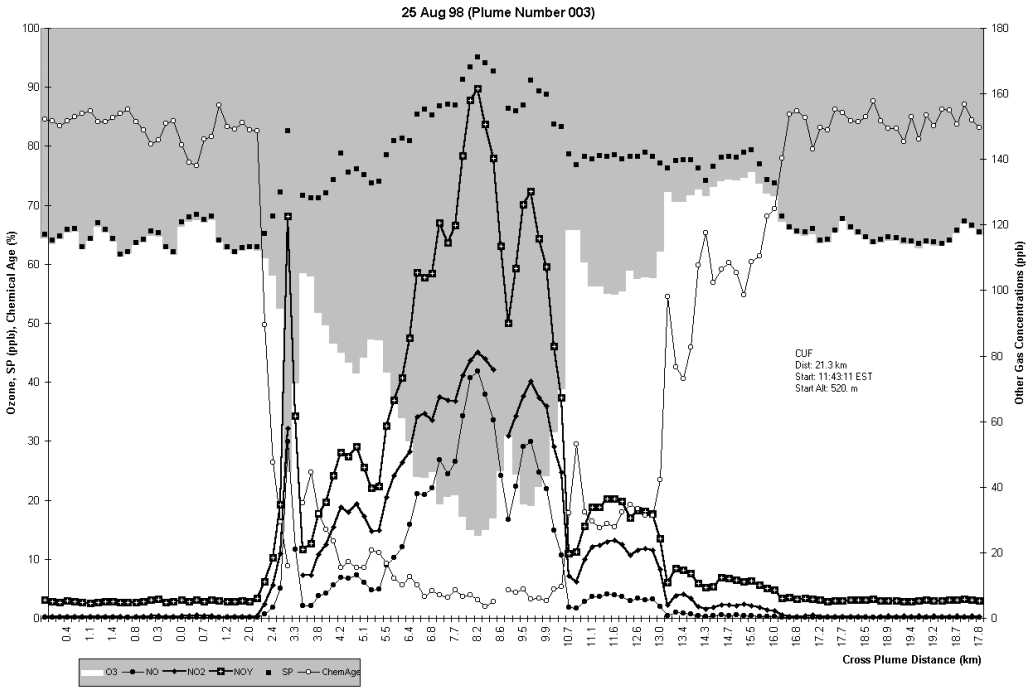

Fig. 4. Measured CUF plume cross section at 21 km downwind. These data were used to illustrate the influences of averaging time on apparent NO production rate.

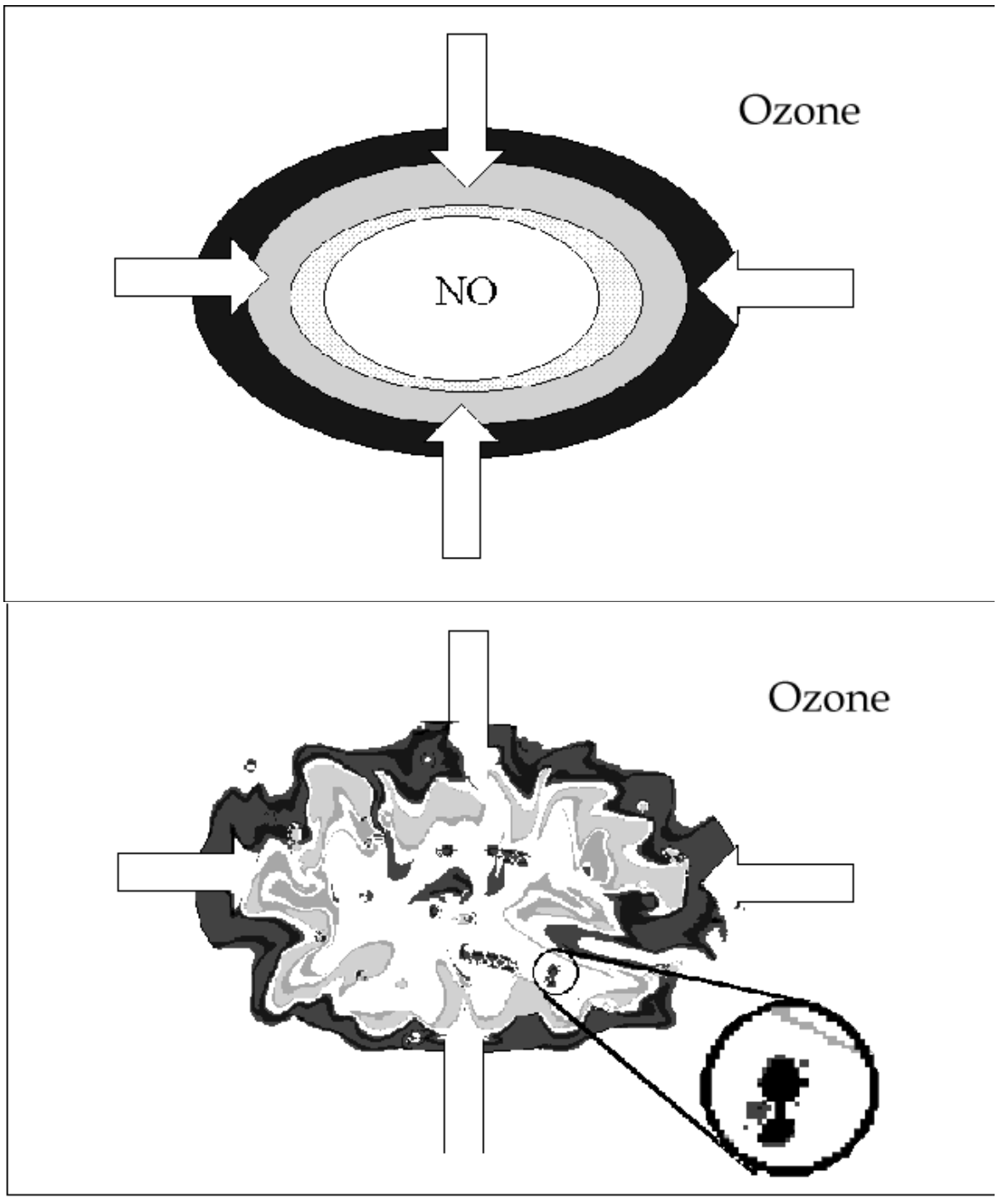

Fig. 5. Schematics of elevated NO_x plume dispersion. Over a one-hour time period (a) the effects of small scale turbulence average out and a Gaussian plume representation is approached. In an instantaneous plume (b) the small scale turbulence creates parcels of concentrated flue gas and highly dilute flue gas next to each other.

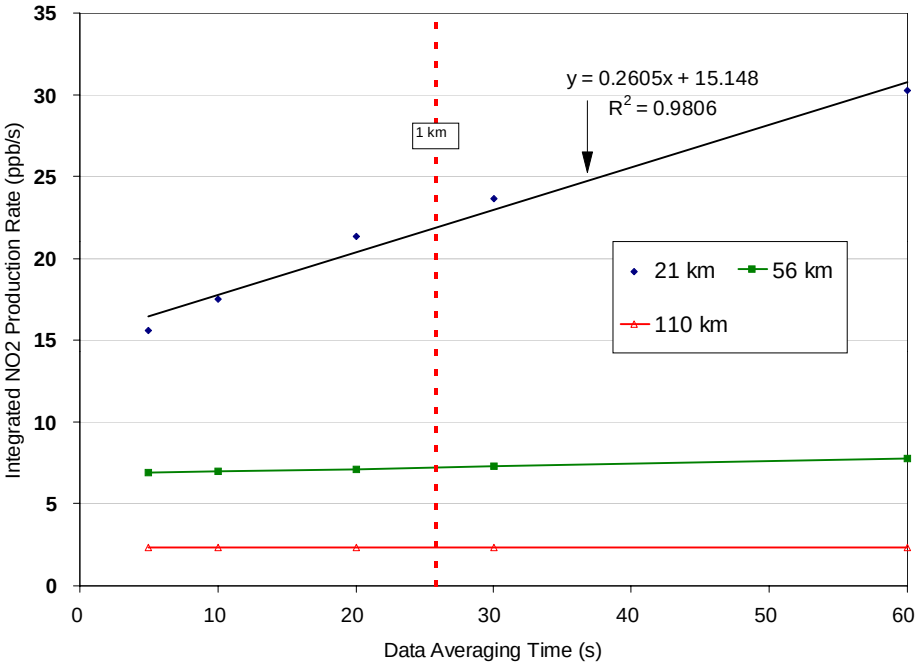

Fig. 6. Sensitivity of computed NO_2 production rate to the averaging time applied to NO and O_3 mixing ratio data.

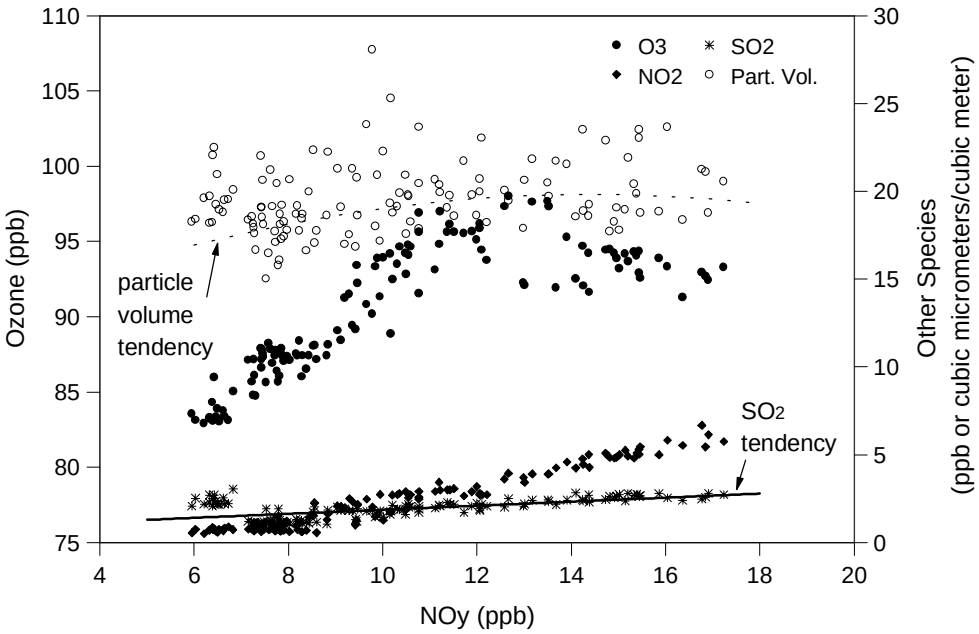

Fig. 7. Plume composition versus NO_y at 110 km downwind on 25 August 1998.

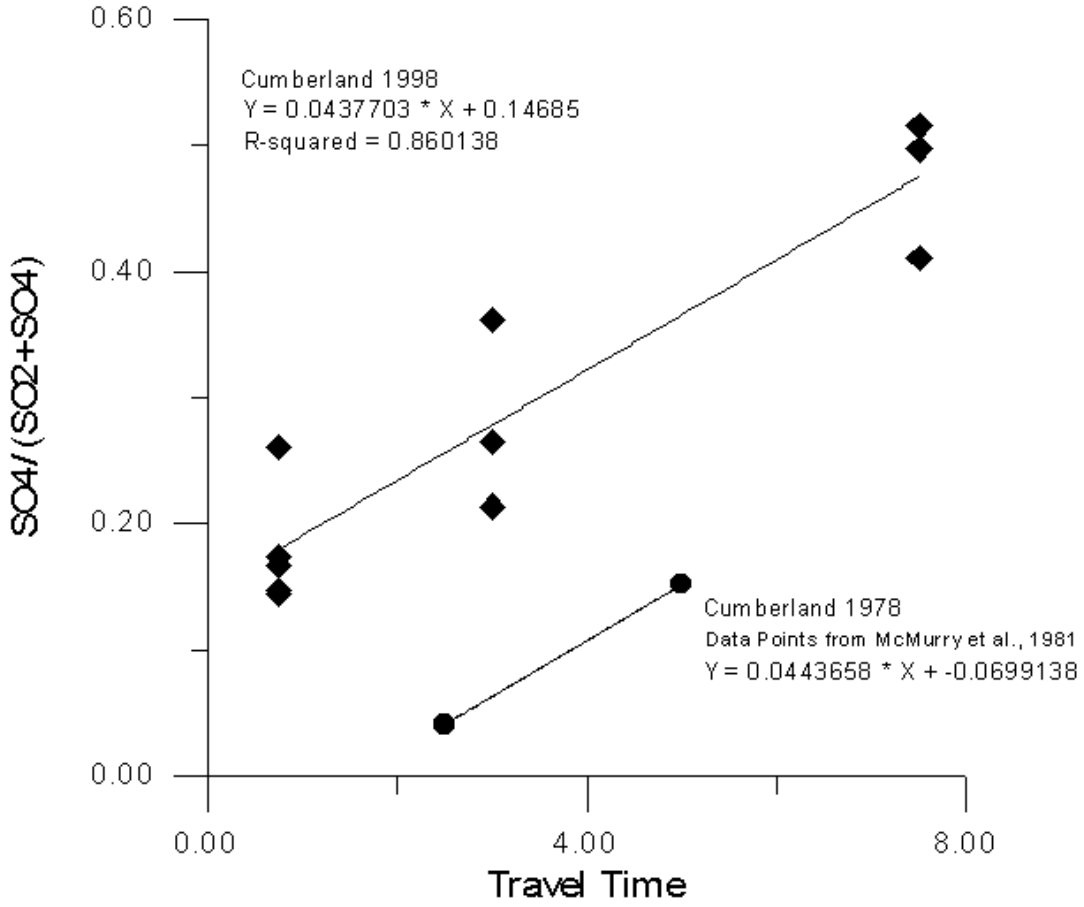

Fig. 8. The fractional abundance of SO_4^{-2}, estimated from the particle size distribution, plotted versus travel time for the 1978 and 1998 CUF data sets. The slope of the lines represents an estimated rate for $SO_2 \Rightarrow SO_4^{-2}$ conversion.